nature materials

ARTICLES

PUBLISHED ONLINE: 16 NOVEMBER 2015 | DOI: 10.1038/NMAT4484

A magnetic protein biocompass

Siying Qin[1†], Hang Yin[1†], Celi Yang[1], Yunfeng Dou[1], Zhongmin Liu[2], Peng Zhang[3], He Yu[4], Yulong Huang[5], Jing Feng[3], Junfeng Hao[6], Jia Hao[1], Lizong Deng[3], Xiyun Yan[3], Xiaoli Dong[5], Zhongxian Zhao[5], Taijiao Jiang[3], Hong-Wei Wang[2], Shu-Jin Luo[4] and Can Xie[1*]

The notion that animals can detect the Earth's magnetic field was once ridiculed, but is now well established. Yet the biological nature of such magnetosensing phenomenon remains unknown. Here, we report a putative magnetic receptor (*Drosophila* CG8198, here named MagR) and a multimeric magnetosensing rod-like protein complex, identified by theoretical postulation and genome-wide screening, and validated with cellular, biochemical, structural and biophysical methods. The magnetosensing complex consists of the identified putative magnetoreceptor and known magnetoreception-related photoreceptor cryptochromes (Cry), has the attributes of both Cry- and iron-based systems, and exhibits spontaneous alignment in magnetic fields, including that of the Earth. Such a protein complex may form the basis of magnetoreception in animals, and may lead to applications across multiple fields.

Magnetic sensing, or the ability to detect the Earth's magnetic field (hereafter magnetoreception), is one of the most controversial animal senses. Many species across all major phyla sense magnetic fields for the purpose of orientation and/or to navigate and migrate over long distances[1,2]. Monarch butterflies[3], salmon[4], lobsters[5,6], bats[7], the mole rat[8,9], and migratory birds[2,10] can perceive navigation cues from geomagnetic fields. Many other species, such as the marine nudibranch mollusk (*Tritonia diomedea*)[11] and the magnetic termite (*Amitermes meridionalis*)[12], use magnetic information to guide and orient their bodies or inhabitant structures (for example, mounds and nests). The existence of a human magnetic sense remains controversial[13,14] but geomagnetic fields are thought to affect the light sensitivity of the human visual system[15]. Definitive identification of a magnetic receptor and comprehensive understanding of how animals sense magnetic fields will inspire innovation in technology across different fields.

Several models have been proposed to explain the nature of magnetoreception[16]. The chemical compass model was pioneered by Schulten[17–19], and later detailed by many others[20–26]. Cryptochromes (Cry), a class of flavoprotein closely related to photolyases, remain the best biochemical magnetoreceptor candidates and have been reported to 'perceive' geomagnetic information via the quantum spin dynamics of a radical-pair reaction initiated by light[24,25,27–29]. The Cry-deficient *Drosophila melanogaster*, which does not show magnetosensitive behaviour, represented the first solid experimental evidence that Cry is necessary for the magnetosensitive pathway in *Drosophila*[30,31]. The response of Cry to magnetic fields via radical pairs may be used to perceive inclination information from a geomagnetic field; however, theoretically it cannot form the basis of a polarity compass. It is thus likely that there exists another partner protein complementary to Cry that enables polarity sensing of geomagnetic fields in some animals.

Ferrimagnetism has been proposed as an enabler of a natural compass system consistent with polarity-and inclination-guided behaviour in animals[32–39]. This hypothesis requires magnetic minerals, for example magnetite, to act as a biomagnetic compass for receiving and responding to geomagnetic cues. However, the identification of such ferrimagnetic sensors (organs or receptor genes) in organisms has been troublesome. Although several magnetite-containing organs or cells from animals have been reported[35,37]—including the upper beak in homing pigeons, chickens and European robins, the superior colliculus of the Zambian mole rat[8] and olfactory epithelial cells in rainbow trout[37]—these have proved irrelevant to magnetoreception[40], or lack validation.

The magnetite-based and radical-pair-reaction-based chemical models both have credible theoretical and experimental foundations, and may not be mutually exclusive; however, evidence from different species tends to favour one hypothesis over the other. Magnetic senses are widespread in animals; some animals appear to detect both the direction and the intensity of the geomagnetic field, some perceive its inclination, and some may use all these navigation cues. Therefore, the existence of multiple mechanisms and separate magnetosensors is possible[41]. Crucial questions are whether phylogenetically distant animals utilize a universal receptor to sense magnetic fields but decode them differently, and the possibility of a missing component in the Cry-based magnetoreception system.

Here, we identified a candidate compass protein using *in silico* genome-wide screening followed by experimental validation. This putative magnetoreceptor protein (MagR) forms a rod-like complex with Cry, and co-localizes with Cry in the pigeon retina. It has appealing structural and magnetic features, which

[1]State Key Laboratory of Membrane Biology, Laboratory of Molecular Biophysics, School of Life Sciences, Peking University, Beijing 100871, China. [2]Ministry of Education Key Laboratory of Protein Science, Center for Structural Biology, Tsinghua-Peking Center for Life Sciences, School of Life Sciences, Tsinghua University, Beijing 100084, China. [3]Key Laboratory of Protein & Peptide Pharmaceuticals, Institute of Biophysics, Chinese Academy of Sciences, Beijing 100101, China. [4]School of Life Sciences, Peking-Tsinghua Center for Life Sciences, Peking University, Beijing 100871, China. [5]Institute of Physics and Beijing National Laboratory for Condensed Matter Physics, Chinese Academy of Sciences, Beijing 100190, China. [6]Center for Experimental Animal Research, Institute of Biophysics, Chinese Academy of Sciences, Beijing 100101, China. †These authors contributed equally to this work.
*e-mail: canxie@pku.edu.cn

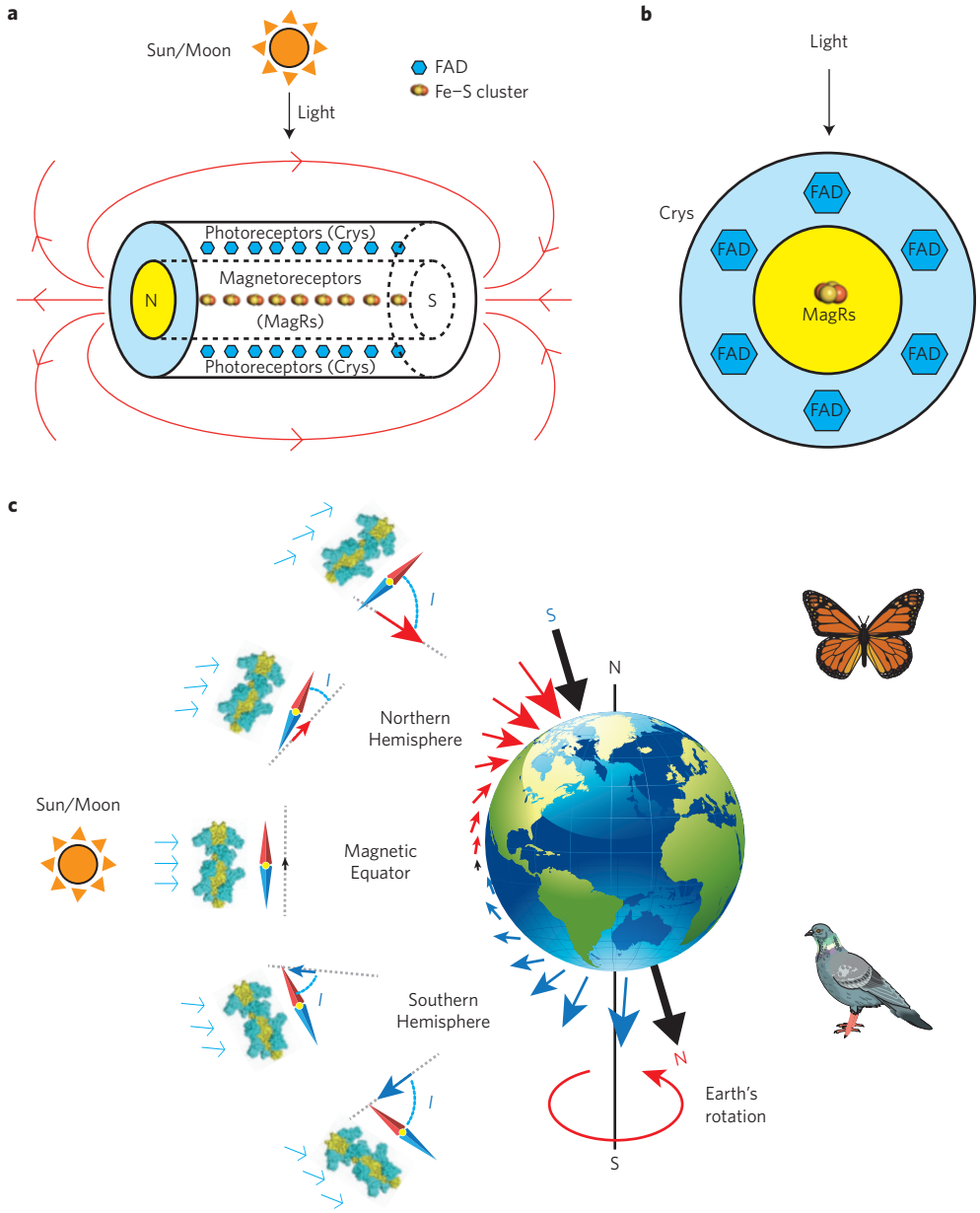

Figure 1 | The biocompass model of animal magnetoreception and navigation. a, A nanoscale Cry/MagR magnetosensor complex with intrinsic magnetic polarity acts as a light-dependent biocompass. Linear polymerization of Fe–S cluster-containing magnetoreceptors (MagR) leads to the formation of a rod-like biocompass at the centre (core, yellow), surrounded by photoreceptive cryptochromes (Cry; outer layer, cyan). **b**, Cross-section of **a**, indicating that electron transportation from the FAD group in Cry to the Fe–S cluster in MagR upon light stimulation may be possible. **c**, The biocompass model of magnetoreception. In animal navigation systems, the Cry/MagR magnetosensor complex may act as a biological compass that perceives information from the Earth's geomagnetic field, such as polarity (as with a conventional compass), intensity and inclination. The surface representation of the Cry/MagR structure (cyan and yellow) has been validated by EM in this study (Figs 2 and 3). The intrinsic magnetic moment of the magnetosensor may form a polarity compass for the sensing of directional information from the Earth's geomagnetic field. The capability to detect the intensity and the spontaneous alignment of the magnetosensor in magnetic fields (as shown on the left-hand side, and further elucidated in Fig. 5a,b), may form the basis of an intensity sensor and inclination compass. Earth's magnetic poles (black arrows) are offset from the axis of rotation (black line). The inclination angle (labelled as 'I') and intensity of the field are indicated by the direction and length of the arrows (red in the Northern Hemisphere and blue in the Southern Hemisphere). MagR and Cry/MagR magnetosensors from two species, monarch butterfly (*Danaus plexippus*, upper right) and pigeon (*Columba livia*, lower right), were tested in this study, highlighting the evolutionarily conserved biocompass model.

are of considerable biological interest and could lead to a range of applications.

The biocompass model of magnetoreception

Different from traditional approaches, in this study we present a strategy that combines theoretical postulation, genome-wide screening, computational modelling and experimental validation in an attempt to reveal a fundamental mechanism for animal magnetic sensing. The theoretical framework was developed on the basis of the following concepts. First, we predict the existence of a protein which forms a magnetic entity (designated MagR) that interacts with Cry and functions as the actual magnetoreceptor (Fig. 1a,b). There are three main strongly magnetic materials known in biological systems: ferrimagnetic minerals (including iron–nickel

oxides), iron-binding proteins, and iron–sulphur cluster proteins. Iron–sulphur cluster proteins play critical roles in numerous cellular functions, especially electron transportation (in which Cry may be involved), and can possess strong magnetic properties, which make them one of the most likely candidates for MagR. We further propose a light–magnetism-coupled magnetoreception model having the attributes of both the magnetic properties of a Fe–S protein and the light-dependent properties of a cryptochrome. Second, to sense the Earth's relatively weak magnetic field and to serve as a biological compass that senses inclination, linear polymerization of MagR may be required. Therefore, a magnetosensitive nanoscale biocompass would be assembled by the combination of photoreceptors (Cry) and magnetoreceptors (MagR), a complex that we define as the magnetosensor (Fig. 1a). Third, the coupling of light and magnetoreception may be due to the interaction between Cry and MagR (Fig. 1a,b), or light-stimulated Cry may be required for biocompass formation or regulation. Fourth, to explain how some animals sense the direction of a geomagnetic field, the nanoscale magnetosensor may have an intrinsic magnetic moment (Fig. 1a). Using this theoretical framework, we began our search for MagR via a genomic screening approach, and conducted biochemical and functional experiments to test and build a three-dimensional (3D) structural model of a protein magnetosensor.

A genome-wide search for MagR

In recognition of the critical role of Cry in the magnetosensitive pathway in fruit flies, we conducted *in silico* screening in the well-annotated genome of *D. melanogaster* to identify iron-containing protein(s) that may interact with *Drosophila* Cry (dCry) (Fig. 2a). A MagR protein fitting our hypothesized magnetoreception theory should have the following characteristics: allow for the binding of magnetic minerals, of which iron or iron–sulphur clusters are the natural choice, a gene-expression profile in the brain (or eyes) in recognition of the involvement of Cry in light-dependent magnetoreception and its expression in retina and brain[42], and the capability of forming a polymeric complex with dCry.

From the fruit-fly genome assembly (BDGP5), 199 iron-binding proteins were selected (Supplementary Table 1), 132 of which have high levels of expression in the head (including brain and eyes, Supplementary Table 2). Because biological tissue is essentially transparent to magnetic fields, there is no need for the putative magnetosensor to be located on the cell surface[16]. We postulated that the magnetosensor complex might be intracellular because dCry is cytoplasmically located[43] and none of the Cry we tested (Supplementary Table 5) are membrane-located. Applying these criteria, the range of candidate proteins was reduced to 98 (Supplementary Table 3). Based on an extensive review of the literature, we then cautiously chose the top 14 most likely candidate proteins (Supplementary Table 4) for downstream tests to determine whether any forms a stable protein complex with dCry.

Experimental identification of MagR

Double tags and tandem co-purification procedures were used to check which candidate proteins interact with dCry and form a protein complex (Fig. 2b). Nine of the selected 14 MagR candidates had confirmed expression in *Drosophila* heads by polymerase chain reaction with reverse transcription (RT–PCR) and were co-expressed with dCry. Only one candidate, CG8198 (Lethal (1) G0136), exhibited stable interaction with dCry (Fig. 2c) and co-purified with dCry in the presence of light and a magnetic field (see Methods for details).

Drosophila CG8198 is the homologue of the bacterial iron–sulphur cluster assembly IscA1, whose function in *Drosophila* remains unclear. Intriguingly, the only available study reported that inhibition of CG8198 expression resulted in disruption of circadian behaviour in the fruit fly[44]. As Cry is known to contribute to circadian-rhythm resetting and photosensitivity[45,46], crosstalk between magnetoreception, photosensitivity and circadian behaviour is possible[47]. We rename CG8198 as the putative magnetoreceptor in *Drosophila* (dMagR), and designate the protein complex formed by Cry and MagR as a putative magnetosensor.

Comparative genomic studies showed that both genes, *cry* and *magr*, are present in the genomes of almost all animal species (Supplementary Figs 1 and 2). Animals have several classes of cryptochromes with various functions, including core elements of circadian clockwork, photoreceptors, and unknown function. We tested the formation of a complex between Cry and MagR in six selected species (fruit fly, monarch butterfly, pigeon, mole rat, minke whale and human; Supplementary Table 5) using the co-purification procedures described above and in Methods. Results suggest that Cry/MagR complex formation is conserved across phyla. In those animals with several classes of Cry (Supplementary Fig. 2), only one Cry complexes with MagR, corroborating the specificity of the Cry/MagR interaction (some representative species are shown in Supplementary Table 5, Fig. 2c and Supplementary Fig. 3). The ratio of Cry and MagR may vary in different species and even in different protein preparations (Fig. 2c and Supplementary Fig. 3), indicating dynamic complex formation.

Structural characterization of MagR and Cry/MagR

A large hydrodynamic radius of both the purified MagR protein and the MagR/Cry complex appeared in size-exclusion chromatography (Superose 6 Increase 10/300, GE Healthcare), suggesting the occurrence of polymerization (Fig. 2d,f) and in contrast to the formation of dimers and monomers of purified Cry protein alone (Supplementary Fig. 7a,b). The polymerization or self-assembly potential of MagR is a critical feature in the magnetosensing system, which may provide a scaling-up mechanism for biological macromolecules, effectively amplifying and utilizing the rather weak magnetic cues from the Earth's magnetic field (0.3–0.65 Gauss (G), or 0.03–0.065 mT; ref. 48). The two purified proteins eluted together in size-exclusion chromatography, further confirming the stable protein interaction between MagR and Cry (Fig. 2f). The fluorescence emission spectrum of the purified yellow-to-brown coloured protein complex indicated the presence of FAD and the binding of iron (Supplementary Fig. 4).

Electron microscopy (EM) was used to further determine the structure of the Cry/MagR complex as represented by the putative pigeon (*Columba livia*) magnetosensor, which formed the most stable complex among tested species (Fig. 2c and Supplementary Fig. 3). MagR polymer and Cry4 alone were also visualized by EM as controls, and to rationalise the structural architecture of the Cry/MagR complex. Briefly, clMagR, clCry4 and clCry4/clMagR complexes were purified to homogeneity by size-exclusion chromatography (Fig. 2d,f and Supplementary Fig. 7), deposited on EM grids with or without an enhanced magnetic field (Supplementary Fig. 5), stained with uranyl acetate, and then inspected by EM (Supplementary Figs 6 and 7). Five main classes of Cry/MagR complexes were visualized by overall shape (classes 1–5), and three groups were classified according to size and structural features (groups 1–3; Fig. 2g–k and Supplementary Fig. 8). For each class, representative two-dimensional averages were shown, and the structural features were summarized and illustrated as cartoons (Fig. 2g–k). EM image classes 1 and 2 (group 1) of the Cry/MagR complex share common features such as smaller diameters and a papillose surface (Fig. 2g,h), and resemble the MagR polymer structure (Fig. 2e). In contrast, classes 3 and 4 (group 2) of the Cry/MagR complex have larger diameters and apparent protruding spikes (Fig. 2i,j). Taking into account the organization and assembly pattern of these two proteins in the proposed model (Fig. 1a,b) and the MagR polymer structure as a reference, we

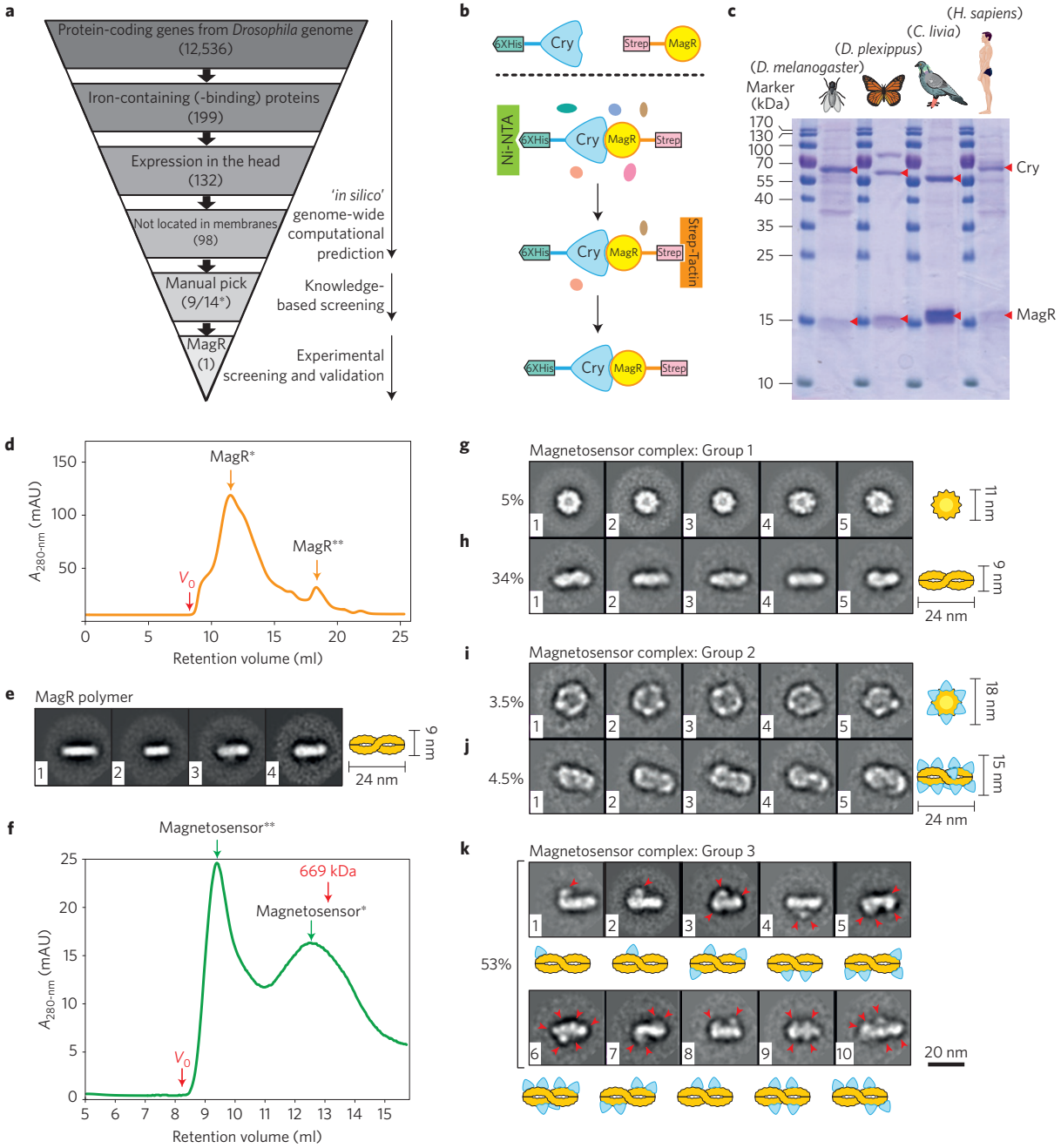

Figure 2 | Genome-wide search, experimental validation and structural characterization of the magnetoreceptor MagR. a, Procedure for the genome-wide search for the magnetoreceptor MagR, including three rounds of '*in silico*' screening, one round of knowledge-based screening and one round of experimental screening. *: Nine out of fourteen candidates confirmed strong expression in the *Drosophila* head and were further screened for complex formation with Cry. **b**, Schematic cartoon showing experimental screening based on the interaction between cryptochrome (cyan) and MagR candidates (yellow). **c**, Cry/MagR complex co-purification from four representative species (fruit fly: *Drosophila melanogaster*; monarch butterfly: *Danaus plexippus*; pigeon: *Columba livia* and human: *Homo sapiens*). Arrows show purified Cry (upper) and MagR (lower) in SDS–PAGE. **d**, Size-exclusion chromatography purification of pigeon MagR protein. (mAU are milliabsorbance units at 280 nm; *: protein fraction in this peak contains MagR polymer used for EM structure determination; **: MagR protein that is invisible under EM, presumably owing to the protein's size and molecular weight (14.5 kDa)). **e**, Negative staining EM structure of pigeon MagR polymer. The proposed double-helix rod-like shape of the MagR polymer (yellow) is shown as a cartoon. **f**, Size-exclusion chromatography purification of the pigeon Cry/MagR complex. (*: protein fraction in this peak corresponds to the isolated magnetosensor complex used for EM structure determination; **: protein aggregation, presumably due to the magnetic attraction among magnetosensor complexes; see Supplementary Fig. 6). **g**–**k**, Negative-staining EM structure of the pigeon magnetosensor complex. All two-dimensional averages can be classified into five classes. Structural features of each class are summarized, and proposed structural architectures are illustrated as cartoons (Cry coloured in cyan, MagR coloured in yellow). **g**–**h**, Group-1 particles representing the top (**g**) and side (**h**) views of the rod-like magnetosensor core structure, presumably formed by MagR. The double-helical structure was clearly seen from negative-staining EM averages. **i**,**j**, Group-2 particles representing the top (**i**) and side (**j**) views of the complete magnetosensor structure, with Cry fully loaded onto the double-helical MagR core. **k**, Group-3 particles showing the dynamics of the Cry/MagR magnetosensor structure. The resolution of the EM structures ranges between 22 and 25 Å. Red arrows show Cry binding to the MagR core structure.

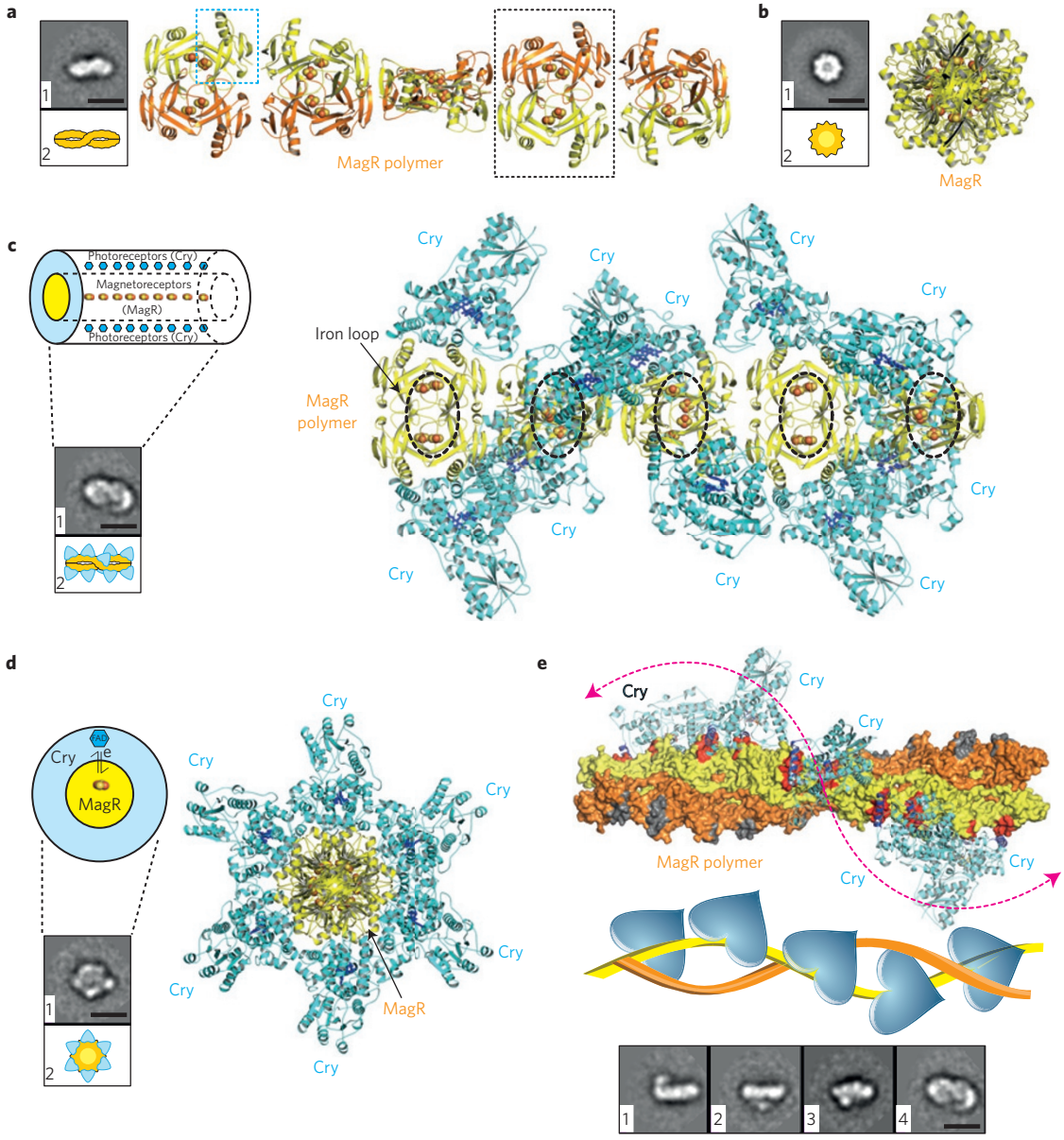

Figure 3 | Molecular modelling bridges the biocompass model and the EM structures. a,**b**, MagR assembled as a rod-like structure. Side (**a**) and top (**b**) views of a double-helical arrangement of 20 MagR molecules, and comparison between EM structure (left) and molecular model (right). Dotted boxes show one MagR monomer (yellow) and four MagR molecules (yellow and orange) comprising a disk-like unit (black), with four Fe–S clusters in the middle forming an iron loop. MagR molecules are coloured yellow and orange to emphasize the double-helical assembly. **c**,**d**, The complete structural model of the Cry/MagR magnetosensor. Side (**c**) and top (**d**) views of the magnetosensor, with ten Cry molecules (cyan) fully loaded to the MagR core (yellow). Comparisons between molecular model (right), light-dependent biocompass model (upper left) and EM structure (lower left) are shown. FADs in Cry are shown as blue sticks and Fe–S clusters in MagR are shown as spheres. The 'iron-loop' structures of the Fe–S cluster arrangement are highlighted with dashed black ovals in **c**. **e**, Proposed structural dynamics (detailed, top; coarse-grained, middle) based on the molecular model and EM structure of the magnetosensor. MagR is coloured yellow and orange to emphasize the double-helical assembly. Five Cry molecules are coloured cyan, with the magenta dotted line showing that the Cry molecules are helically located on the outer layer. The conserved helix–helix interactions between Cry and MagR are coloured red and grey in MagR, and blue in Cry. Four typical EM averages (bottom) exemplify the dynamics of Cry binding to MagR.

suggest that group 2 (Fig. 2i,j) represents the complete Cry/MagR complex structure, which is characterized by an outer layer helically surrounded by Cry and a rod-like core structure formed by MagR polymerization; group 1 (Fig. 2g,h) instead represents the sole MagR core structure with Cry dissociated from MagR, consistent with the MagR polymer configuration. Partially dissociated Cry 'rods' were also observed (group 3, Fig. 2k). Consistent with our model, all different statuses and compositions of the proposed magnetosensor system were observed under EM, suggesting a highly dynamic feature of the protein complex.

In the EM experiments with the Cry/MagR complex, the rod-like particles as predicted with our model appeared as majority populations in the EM field (91.5%, Fig. 2h,j,k). In addition, two classes of particles with round-disk-like shapes and different diameters were observed (8.5%, Fig. 2g,i). We propose that these round-disk-like and rod-like particles represent two different views of the same kind of particles on the grid: cross-section (Fig. 2g,i) and longitudinal section (Fig. 2h,j). Differences in the orientation seem reasonable considering how a rod-like object settles on a flat surface. The structure of the monarch butterfly dpCry1/dpMagR complex

also has a rod-like shape and similarity to the pigeon clCry4/clMagR complex under EM (Supplementary Fig. 9). This may indicate a conserved structural architecture for the Cry/MagR complex in animals.

Molecular modelling of Cry/MagR complex structure

The computational approaches of 3D homology modelling, *in silico* assembly and molecular docking, were combined to interpret the EM structure and determine the assembly of the Cry/MagR complex at the molecular level (see Methods for details). Briefly, a 3D homology model of pigeon clMagR was generated based on the structure of the homologous bacterial iron–sulphur cluster protein IscA (PDB ID: 1R94; ref. 49). The crystal packing pattern in IscA revealed a double-helical linear polymerization with metal irons located at the centre (Supplementary Fig. 10), in good agreement with the helical rod-like core structure observed in our proposed MagR assembly pattern observed under EM (Fig. 2h). The top view of this rod-like structural model has a round-disk shape (consistent with the EM structure; Fig. 2g) and validates our assumption that the rod-like and round-disk-like shapes indeed represent two orientations of the same structure.

We then modelled the 'core' structure (clMagR polymer) according to the crystal packing pattern of the IscA homologue (Fig. 3a,b and Supplementary Fig. 10). The group-2 EM particles have a large diameter and radiating spikes, which may indicate the presence of multiple cryptochromes around the MagR core structure. Knowledge-based molecular docking was applied: full-length Cry crystal units (PDB ID: 4GU5; ref. 50) were docked onto the rod-like clMagR core structure one by one, via alignment of the two conserved helices of each Cry structure to the 'helix–helix' structure (Supplementary Fig. 11a) that forms the critical crystal packing interface, as shown by the homologous IscA structure (Supplementary Fig. 11b–d) and the molecular ratio of clCry: clMagR is 1:2 in the model. The complete Cry/MagR complex structure assembled into a rod-like polymer with the magnetoreceptive MagR located in the centre, which may sense the magnetic field, and light-receptive helical Cry in the peripheral layer functioning as antennas that may receive light stimuli (Fig. 3c,d). The cross-sectional view of the Cry/MagR complex formed a hexagonal snow-flake-like shape, representing the light–magnetic-field interaction proposed in Fig. 1b. The projection with the highest cross-correlation coefficient corresponded to the orientation of the final computation structural model of the Cry/MagR complex (Fig. 3a–d), revealing that the EM structure is in excellent agreement with our Cry/MagR structural model.

The structural model of the putative magnetosensor was validated by biochemical and mutagenesis studies. Deleting the conserved C-terminal helix of Cry greatly decreased Cry/MagR complex formation (Supplementary Fig. 12a,b), indicating that the Cry–MagR interface proposed in our structural model is essential. Removing the Fe–S cluster in MagR nearly abolished the Cry–MagR interaction (Supplementary Fig. 12c–e), suggesting that the Fe–S cluster may be critical for the assembly of the Cry/MagR complex. The MagR core structure was interrupted after introduction of another component in the N-terminus of MagR, suggesting that the assembly of the MagR polymer is compact and intolerant to disturbances (Supplementary Fig. 13).

It is interesting that in the 24-nm rod-like magnetosensor-complex structural model, 20 Fe–S clusters from 20 MagR monomers aligned in the centre (Fig. 3a,c); every four MagR formed a disk-like unit (Fig. 3a) with four Fe–S clusters arranged as an 'iron-loop' circle (Fig. 3c) perpendicular to the longitudinal section of the rod-like magnetosensor complex. We also noticed that the two conserved helices of MagR (coloured red or grey in Fig. 3e) appear on the surface and are arrayed as a ladder in the MagR polymer, forming the main interface with Cry through helix–helix interactions (Fig. 3e and Supplementary Fig. 11). This feature suggests a possible sliding of Cry molecules along a 'ladder' on the surface of the rod-like MagR polymer (Fig. 3e). The Cry/MagR ratio variation in protein preparations may represent a highly dynamic interaction between Cry and MagR.

Theoretically, the assembly of this polymer is not limited by length. However, the observed length under EM is uniform and corresponds to 20–24 nm for both the MagR core (Fig. 2e,h) and the Cry/MagR complex structure (Fig. 2j,k), and is in accordance with the length and size of 20 MagR and 10 Cry according to our structural modelling. This suggests that the assembly of this putative magnetosensor may be tightly regulated (as would be the actual case under physiological conditions).

Expression of MagR and Cry co-localized in the retina

In addition to invertebrate Cry and vertebrate Cry1 and Cry2, nonmammalian vertebrates, such as birds, have Cry4; pigeon clCry4, but not clCry1a, clCry1b and clCry2, was confirmed in our experiments as forming a complex with clMagR. We investigated if the expression of clCry4 and clMagR co-localized in physiological conditions. Antibodies to clCry4 and clMagR were developed, and the expression profile of the putative magnetosensor at tissue and cellular levels was elucidated by immunohistochemical studies (Fig. 4). It has been reported that chicken Cry4 is highly expressed in multiple layers of retina cells[51]. We found that both clMagR and clCry4 are highly expressed and co-localized in pigeon retina, especially in the retinal ganglion cell layer (GCL), inner nuclear layer (INL) and outer nuclear layer (ONL, Fig. 4a–d). The signal intensities of clCry and clMagR expression were relatively strong in the GCL compared with cells in the ONL and INL (Fig. 4e–l). Most retinal ganglion cells show co-localized expression of clCry4 and clMagR, and the nearby nerve fibre layer (NFL) exhibited weaker signals (Fig. 4e–h). Some, but not all cells in the ONL, also showed strong expression of both clCry4 and clMagR (Fig. 4i–l). We noticed that in visual pigment cells (VPCs), clMagR exhibited extended expression whereas the expression of clCry4 was lacking (Fig. 4a–d). The precise identity of immunopositive cells in the ONL and the INL may require further analysis. The co-localization of clCry4 and clMagR in multiple layers of retinal cells is in agreement with previously proposed magnetoreception models in the avian retina, and the slightly different expression of clCry4 and clMagR in specific cells is consistent with our biochemical data showing the dynamics of Cry/MagR complex formation. Considering the reported expression pattern of the neuronal-activity marker c-Fos in retinal ganglion cells in the migratory garden warbler[52], the co-localized expression of our putative magnetosensor (clCry4 and clMagR) in retinal ganglion cells and in the NFL may suggest a potential mechanism for animal magnetoreception (Fig. 4m,n).

Intrinsic magnetic moment of MagR and Cry/MagR

We validated the existence of an intrinsic magnetic moment of the proposed Cry/MagR complex by using four methods: EM imaging, a simple purification procedure of the MagR and Cry/MagR complex with iron beads, protein crystallization experiments, and by directly measuring the magnetic properties of the protein complex in solution. In theory, the flat-sitting orientation of a rod-like complex on the EM grid should be in a fully random pattern under a magnetic field if the particle is not magnetically polarizing. By contrast, we observed significant orientation preferences of the Cry/MagR complex on EM grids, with about 45% of the isolated rod-like protein particles oriented with their long axis roughly parallel to the geomagnetic field. When an enhanced artificial magnetic field (10 G) was applied during EM sample preparation, the fraction of particles parallel to the external magnetic-field lines increased significantly (55%), accompanied by

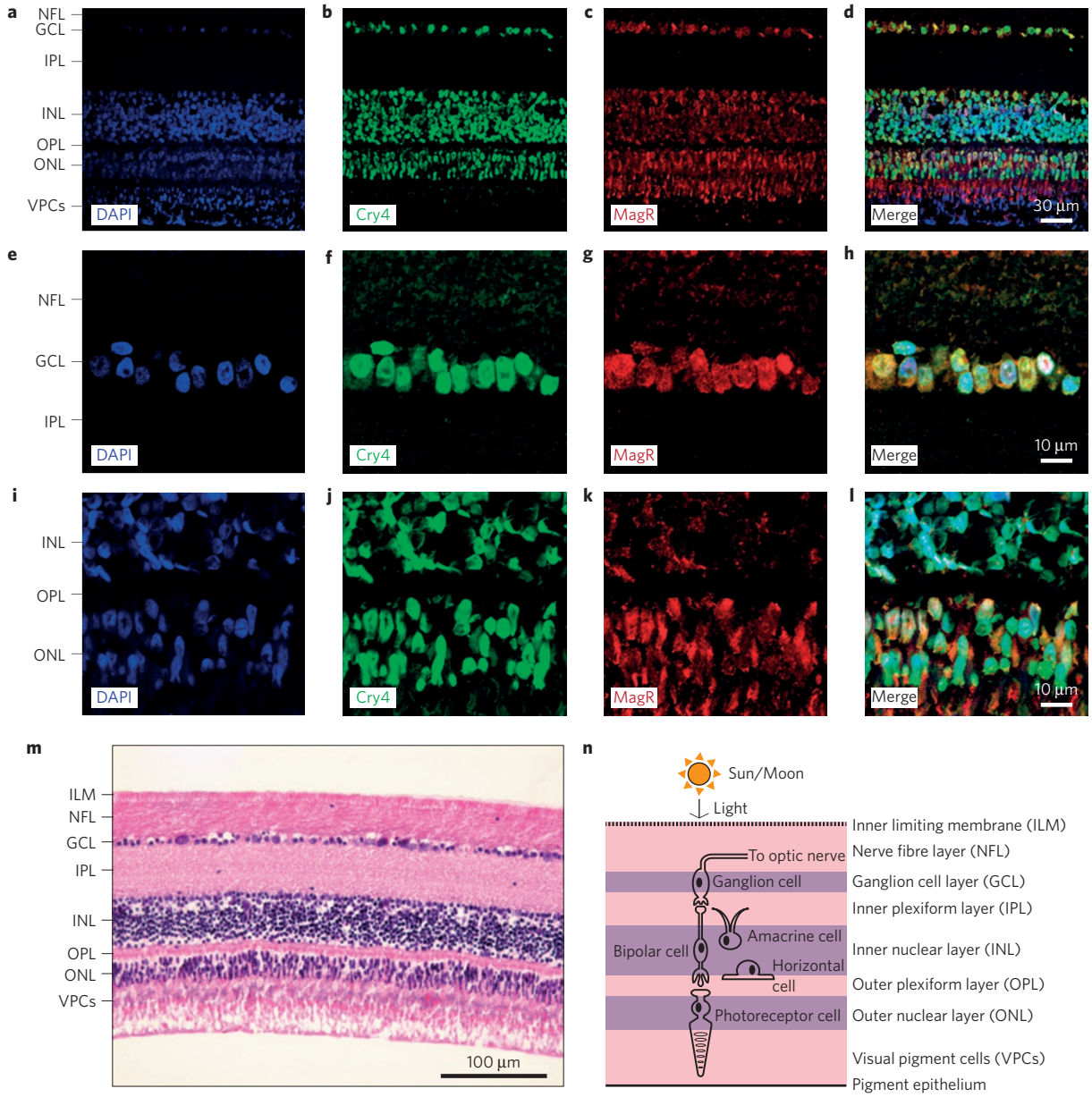

Figure 4 | Expression of MagR and Cry in multilayers of the pigeon retina. Co-localization of Cry4 and MagR in the same 6-µm-thick pigeon retina slice. Immunohistochemical staining showed cell nuclei (blue; DAPI (4′,6-diamidino-2-phenylindole)), clCry4 protein (green) and clMagR (red) in the pigeon retina. Confocal images are shown in **a**–**l**, and histochemical analysis showing the multilayer structure of the pigeon retina as a reference is shown in **m**. **a**–**d**, clCry4 (green) and clMagR (red) expressed in multilayers of the pigeon retina. **e**–**h**, Zoom-in images showing the co-localization of clCry4 and clMagR protein expression in the GCL and the NFL. **i**–**l**, Zoom-in images showing the co-localized expression of clCry4 and clMagR in the INL and the ONL. **m**, Representative H&E-stained pigeon-retina sections. **n**, Schematic representation of the main cell types in the retina.

a decreased population in the vertical direction (Fig. 5a,b and Supplementary Fig. 14), and thus suggesting the capability to detect the intensity of magnetic fields. Because orientation in a magnetic field is continually counteracted by thermal motion, which randomizes the orientations during EM sample preparation[53], the 45–55% orientation preference of our Cry/MagR complex is already statistically indicative of a strong tendency to align itself with geomagnetic or given magnetic fields, even at a nanoscale single-particle level. We also designed a straightforward procedure similar to a pull-down experiment for purification to validate the magnetic features of the MagR protein and the nanoscale Cry/MagR complex in solution. The clMagR protein and/or the clCry4/clMagR protein complex were greatly enriched by non-magnetized iron beads (Fig. 5c), a strong demonstration of the intrinsic magnetic moment proposed for the MagR protein and Cry/MagR complex.

Two types of protein crystals with different morphologies (Fig. 5d) were obtained from several conditions for pigeon clCry4/clMagR and monarch butterfly dpCry1/dpMagR complexes. All crystals exhibited strong magnetic polarity in response to an external magnetic field. Under a light microscope with an artificial magnetic field rotating in the focal plane, we observed complex crystals in the crystallization trays rotating in a synchronous manner (Fig. 5d and Supplementary Movies 1 and 2). In addition, the protein crystals would instantly flip 180° when the approaching magnetic polarity was horizontally inverted, which demonstrates the intrinsic magnetic polarity of the Cry/MagR complex. The magnetic strength of the Cry/MagR complex was so strong that

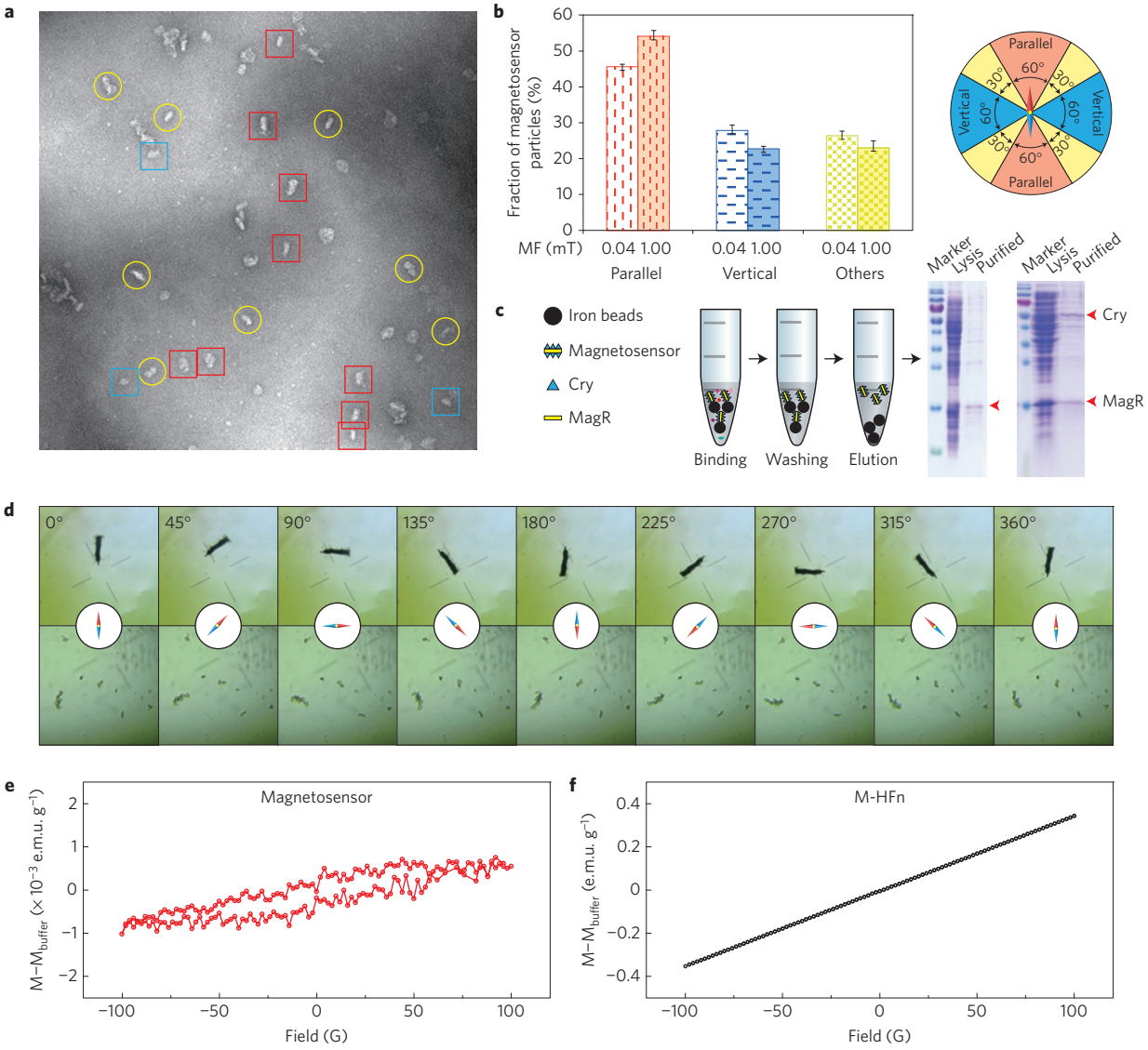

Figure 5 | Intrinsic magnetic polarity of the magnetosensor. a, Representative raw image of the clCry4/clMagR magnetosensor complex prepared under the geomagnetic field (0.4 G, or 0.04 mT). Isolated rod-like particles aligned in parallel, vertical or other intermediate directions with respect to the geomagnetic direction are shown in red boxes, blue boxes and yellow circles, respectively. The definition of parallel, vertical and others is explained in **b** (insert). **b**, The percentage of isolated magnetosensor particles in the three directions corresponding to the geomagnetic field (0.4 G, or 0.04 mT) or to an enhanced external magnetic field (MF) (10 G, or 1 mT). The enhanced external magnetic field is applied vertically to the geomagnetic field. Around 500 particles are randomly picked using EMAN and analysed for each experiment. Results are from three independent experiments; error bars: mean ± s.d. **c**, clMagR (SDS–PAGE, left) and clCry4/clMagR complex (SDS–PAGE, right) can be enriched with iron beads from co-expressed cell lysis by a simple procedure. **d**, Magnetosensor protein crystals exhibited strong intrinsic magnetic polarity and rotated in synchrony with the external magnetic field. Two types of protein crystals, brown-to-black crystal (upper panels) and translucent yellowish crystals (lower panels) are shown. There is only one brown-to-black crystal in one hanging drop, which might be due to the merging of small crystals because of the magnetic dragging force; however, many translucent yellowish crystals may coexist. **e**, Magnetic properties of the clCry4/clMagR magnetosensor complex. Room-temperature magnetization as a function of the field for the clCry4/clMagR magnetosensor complex was obtained by subtracting the contribution of buffer from solution (Supplementary Fig. 16). The presence of a hysteresis loop indicates the ferrimagnetic behaviour of the clCry4/clMagR complex. **f**, Magnetic properties of synthesized magnetite-containing human ferritin (M-HFn) nanoparticles were used as a control. The linear dependence indicates that no ferrimagnetic ordering exists in M-HFn.

crystal handling tools (Hampton, USA) could not be used because the crystals 'fly' out of the solution and stick to iron-made tools. Thus, all tools used in crystallization experiments were customized plastic (Supplementary Fig. 15). We observed that crystals were growing from the clear protein solution in sealed hanging drops in our experiments, which excluded possible air-borne magnetite contamination. To our knowledge, this is the first time that a protein or protein complex has been shown to possess an intrinsic magnetic moment and biocompass-like functionality.

As complicated as biological systems are, they certainly obey and often make ingenious use of physical principles. To explore the physical properties of the protein-based nanostructured Cry/MagR complex, magnetic measurements of clCry4/clMagR (Fig. 5e and Supplementary Fig. 16a,b) were conducted with a commercial magnetometer (Quantum Design magnetic property measurement system, MPMS-XL1). Figure 5e reveals the field dependence of the magnetization of the clCry4/clMagR complex. The complex we identified is ferrimagnetic at room temperature,

with a coercivity of approximately 20 G in magnitude. The two kinks appearing around zero magnetization indicate the existence of two vortex states with opposite directions, similar to the behaviours observed in ferrimagnetic nanorings[54], and in agreement with the here proposed 'iron-loop' hypothesis on the basis of structural modelling (Fig. 3c). In contrast, ferritin, the main intracellular storage form of iron, a spherical protein composed of 24 subunits, fully loaded with around 4,500 iron atoms, shows a linear dependence and no hysteresis in our experiment (Fig. 5f and Supplementary Fig. 16c,d), indicating a non-ferrimagnetic character consistent with previous reports[55]. We propose two possible causes of the intrinsic magnetic feature of this magnetosensor: the linear array of iron atoms and/or a synchronized circular current in the iron loops. To our knowledge, such ferrimagnetic behaviour and vortex states with opposite directions of the clCry4/clMagR protein complex in solution have not been shown previously, and are consistent with our observations (Fig. 5a–d).

Thus far, we are able to unambiguously prove that a specific Fe–S cluster protein in animals interacts with the known magnetoreception-related protein cryptochrome and forms a nanoscale macromolecular complex. It has unique biophysical features and significant biological implications, including the following six. First, the nanoscale protein-complex structure predicted and demonstrated here is evolutionarily conserved from insects to mammals, and has the potential to act as a biological compass for the perception of navigational cues, including geomagnetic fields. Second, the rod-like magnetosensor consists of linearly polymerized, iron-containing putative magnetoreceptors (MagR) helically surrounded by photoreceptors (Cry), and suggests a potential mechanism for the coupling of light and magnetic detection, and (or) even for circadian-rhythm behaviour in some species. Third, the dynamics of the Cry/MagR protein complex and the polymer structure formed by MagR alone may potentially act as a biocompass in the dark in some cell types and animal species, or as a mechanism for light regulation in magnetoreception. For certain species known to be capable of responding to magnetic fields in the dark, the mechanism of the coupling of light and magnetosensing, if it exists, will be worth exploring. Fourth, the co-localized expression of Cry and MagR in the retina, especially in retinal ganglion cells, combined with previously reported neuronal-activity marker c-Fos expression in such cells (ref. 52), may provide clues as to how the signals from navigation cues are delivered to the nervous system. Fifth, the nanoscale biocompass has the tendency to align itself along geomagnetic field lines, and to obtain navigation cues from a geomagnetic field. Last, any disturbance of this alignment may be captured by connected cellular machinery such as the cytoskeleton or ion channels, which would channel information to the downstream neural system forming the animal's magnetic sense (or magnetic 'vision'). In summary, the magnetoreceptor (MagR) and magnetosensor proteins identified here, along with their structural model and functional exploration, represent a novel biocompass-like model and may help resolve the mystery of animal magnetoreception via an innate molecular sensor capable of perceiving and responding to the Earth's magnetic field (Fig. 1c).

Outlook

The Cry/MagR magnetosensor system is largely compatible with century-old animal behaviour studies, the well-established Cry-dependent magnetoreception pathway, and the ferrimagnetism hypothesis. The identification and experimental validation of MagR may be the missing piece of the puzzle as to how Cry leads to cellular- and organism-level responses to magnetic fields and why Cry-deficient fruit flies lose such capability. The biocompass model we present here may serve as a step towards fully uncovering the molecular mechanism of animal navigation and magnetoreception. It has not escaped our notice that the magnetic features of the MagR polymer and Cry/MagR complex may provide a useful tool for the isolation and manipulation of macromolecules with external magnetic fields, give rise to magnetogenetics and inspire numerous potential applications across different fields.

Methods

Methods and any associated references are available in the online version of the paper.

Received 4 August 2015; accepted 21 October 2015; published online 16 November 2015

References

1. Wiltschko, R. & Wiltschko, W. *Magnetic Orientation in Animals* (Springer, 1995).
2. Wiltschko, W. & Wiltschko, R. Magnetic orientation and magnetoreception in birds and other animals. *J. Comp. Physiol.* **191,** 675–693 (2005).
3. Zhan, S., Merlin, C., Boore, J. L. & Reppert, S. M. The monarch butterfly genome yields insights into long-distance migration. *Cell* **147,** 1171–1185 (2011).
4. Quinn, T. Evidence for celestial and magnetic compass orientation in lake migrating sockeye salmon fry. *J. Comp. Physiol.* **137,** 243–248 (1980).
5. Cain, S. D., Boles, L. C., Wang, J. H. & Lohmann, K. J. Magnetic orientation and navigation in marine turtles, lobsters, and molluscs: Concepts and conundrums. *Integr. Comp. Biol.* **45,** 539–546 (2005).
6. Boles, L. C. & Lohmann, K. J. True navigation and magnetic maps in spiny lobsters. *Nature* **421,** 60–63 (2003).
7. Wang, Y., Pan, Y., Parsons, S., Walker, M. & Zhang, S. Bats respond to polarity of a magnetic field. *Proc. Biol. Sci.* **274,** 2901–2905 (2007).
8. Nemec, P., Altmann, J., Marhold, S., Burda, H. & Oelschlager, H. H. Neuroanatomy of magnetoreception: The superior colliculus involved in magnetic orientation in a mammal. *Science* **294,** 366–368 (2001).
9. Marhold, S., Wiltschko, W. & Burda, H. A magnetic polarity compass for direction finding in a subterranean mammal. *Naturwissenschaften* **84,** 421–423 (1997).
10. O' Neill, P. Magnetoreception and baroreception in birds. *Dev. Growth Differ.* **55,** 188–197 (2013).
11. Pavlova, G. A., Glantz, R. M. & Dennis Willows, A. O. Responses to magnetic stimuli recorded in peripheral nerves in the marine nudibranch mollusk *Tritonia diomedea*. *J. Comp. Physiol.* **197,** 979–986 (2011).
12. Jacklyn, P. M. & Munro, U. Evidence for the use of magnetic cues in mound construction by the termite *Amitermes meridionalis* (Isoptera : Termitinae). *Aust. J. Zool.* **50,** 357–368 (2002).
13. Westby, G. W. & Partridge, K. J. Human homing: Still no evidence despite geomagnetic controls. *J. Exp. Biol.* **120,** 325–331 (1986).
14. Baker, R. R. *Human Navigation and the Sixth Sense* (Hodder and Stoughton, 1981).
15. Thoss, F., Bartsch, B., Fritzsche, B., Tellschaft, D. & Thoss, M. The magnetic field sensitivity of the human visual system shows resonance and compass characteristic. *J. Comp. Physiol.* **186,** 1007–1010 (2000).
16. Johnsen, S. & Lohmann, K. J. Magnetoreception in animals. *Phys. Today* **61,** 29–35 (March, 2008).
17. Schulten, K. & Weller, A. Exploring fast electron transfer processes by magnetic fields. *Biophys. J.* **24,** 295–305 (1978).
18. Schulten, K. & Windemuth, A. in *Biophysical Effects of Steady Magnetic Fields* (eds Maret, G., Kiepenheuen, J. & Boccara, N.) 99–106 (Springer, 1986).
19. Mohseni, M., Omar, Y., Engel, G. S. & Plenio, M. B. in *Quantum Effects in Biology* (eds Solov'yov, I. S., Ritz, T., Schulten, K. & Hore, P. J.) Ch. 10, 218–236 (Cambridge Univ. Press, 2014).
20. Ritz, T., Adem, S. & Schulten, K. A model for photoreceptor-based magnetoreception in birds. *Biophys. J.* **78,** 707–718 (2000).
21. Solov'yov, I. A. & Schulten, K. Magnetoreception through cryptochrome may involve superoxide. *Biophys. J.* **96,** 4804–4813 (2009).
22. Solov'yov, I. A., Mouritsen, H. & Schulten, K. Acuity of a cryptochrome and vision-based magnetoreception system in birds. *Biophys. J.* **99,** 40–49 (2010).
23. Cai, J. & Plenio, M. B. Chemical compass model for avian magnetoreception as a quantum coherent device. *Phys. Rev. Lett.* **111,** 230503 (2013).
24. Rodgers, C. T. & Hore, P. J. Chemical magnetoreception in birds: The radical pair mechanism. *Proc. Natl Acad. Sci. USA* **106,** 353–360 (2009).
25. Maeda, K. *et al.* Chemical compass model of avian magnetoreception. *Nature* **453,** 387–390 (2008).

26. Moller, A., Sagasser, S., Wiltschko, W. & Schierwater, B. Retinal cryptochrome in a migratory passerine bird: A possible transducer for the avian magnetic compass. *Naturwissenschaften* **91,** 585–588 (2004).
27. Mouritsen, H. & Ritz, T. Magnetoreception and its use in bird navigation. *Curr. Opin. Neurobiol.* **15,** 406–414 (2005).
28. Ritz, T., Thalau, P., Phillips, J. B., Wiltschko, R. & Wiltschko, W. Resonance effects indicate a radical-pair mechanism for avian magnetic compass. *Nature* **429,** 177–180 (2004).
29. Mouritsen, H. & Hore, P. J. The magnetic retina: Light-dependent and trigeminal magnetoreception in migratory birds. *Curr. Opin. Neurobiol.* **22,** 343–352 (2012).
30. Gegear, R. J., Casselman, A., Waddell, S. & Reppert, S. M. Cryptochrome mediates light-dependent magnetosensitivity in *Drosophila*. *Nature* **454,** 1014–1018 (2008).
31. Gegear, R. J., Foley, L. E., Casselman, A. & Reppert, S. M. Animal cryptochromes mediate magnetoreception by an unconventional photochemical mechanism. *Nature* **463,** 804–807 (2010).
32. Fleissner, G. *et al.* Ultrastructural analysis of a putative magnetoreceptor in the beak of homing pigeons. *J. Comp. Neurol.* **458,** 350–360 (2003).
33. Fleissner, G., Stahl, B., Thalau, P., Falkenberg, G. & Fleissner, G. A novel concept of Fe-mineral-based magnetoreception: Histological and physicochemical data from the upper beak of homing pigeons. *Naturwissenschaften* **94,** 631–642 (2007).
34. Falkenberg, G. *et al.* Avian magnetoreception: Elaborate iron mineral containing dendrites in the upper beak seem to be a common feature of birds. *PLoS ONE* **5,** e9231 (2010).
35. Hanzlik, M. *et al.* Superparamagnetic magnetite in the upper beak tissue of homing pigeons. *Biometals* **13,** 325–331 (2000).
36. Kirschvink, J. L. & Gould, J. L. Biogenic magnetite as a basis for magnetic field detection in animals. *Biosystems* **13,** 181–201 (1981).
37. Eder, S. H. *et al.* Magnetic characterization of isolated candidate vertebrate magnetoreceptor cells. *Proc. Natl Acad. Sci. USA* **109,** 12022–12027 (2012).
38. Cadiou, H. & McNaughton, P. A. Avian magnetite-based magnetoreception: A physiologist's perspective. *J. R. Soc. Interface* **7,** S193-205 (2010).
39. Mann, S., Sparks, N. H., Walker, M. M. & Kirschvink, J. L. Ultrastructure, morphology and organization of biogenic magnetite from sockeye salmon, *Oncorhynchus nerka*: Implications for magnetoreception. *J. Exp. Biol.* **140,** 35–49 (1988).
40. Treiber, C. D. *et al.* Clusters of iron-rich cells in the upper beak of pigeons are macrophages not magnetosensitive neurons. *Nature* **484,** 367–370 (2012).
41. Lohmann, K. J., Lohmann, C. M. & Putman, N. F. Magnetic maps in animals: Nature's GPS. *J. Exp. Biol.* **210,** 3697–3705 (2007).
42. Yoshii, T., Todo, T., Wulbeck, C., Stanewsky, R. & Helfrich-Forster, C. Cryptochrome is present in the compound eyes and a subset of *Drosophila*'s clock neurons. *J. Comp. Neurol.* **508,** 952–966 (2008).
43. Ceriani, M. F. *et al.* Light-dependent sequestration of TIMELESS by CRYPTOCHROME. *Science* **285,** 553–556 (1999).
44. Mandilaras, K. & Missirlis, F. Genes for iron metabolism influence circadian rhythms in *Drosophila melanogaster*. *Metallomics* **4,** 928–936 (2012).
45. Chaves, I. *et al.* The cryptochromes: Blue light photoreceptors in plants and animals. *Annu. Rev. Plant Biol.* **62,** 335–364 (2011).
46. Zhu, H. *et al.* Cryptochromes define a novel circadian clock mechanism in monarch butterflies that may underlie sun compass navigation. *PLoS Biol.* **6,** e4 (2008).
47. Yoshii, T., Ahmad, M. & Helfrich-Forster, C. Cryptochrome mediates light-dependent magnetosensitivity of *Drosophila*'s circadian clock. *PLoS Biol.* **7,** e1000086 (2009).
48. Solov'yov, I. A. & Greiner, W. Micromagnetic insight into a magnetoreceptor in birds: Existence of magnetic field amplifiers in the beak. *Phys. Rev. E* **80,** 041919 (2009).
49. Bilder, P. W., Ding, H. & Newcomer, M. E. Crystal structure of the ancient, Fe–S scaffold IscA reveals a novel protein fold. *Biochemistry* **43,** 133–139 (2004).
50. Zoltowski, B. D. *et al.* Structure of full-length *Drosophila* cryptochrome. *Nature* **480,** 396–399 (2011).
51. Watari, R. *et al.* Light-dependent structural change of chicken retinal Cryptochrome4. *J. Biol. Chem.* **287,** 42634–42641 (2012).
52. Mouritsen, H. *et al.* Cryptochromes and neuronal-activity markers colocalize in the retina of migratory birds during magnetic orientation. *Proc. Natl Acad. Sci. USA* **101,** 14294–14299 (2004).
53. Schrödinger, E. *What Is Life? with Mind and Matter and Autobiographical Sketches* (Cambridge Univ. Press, 1967).
54. Jia, C. J. *et al.* Large-scale synthesis of single-crystalline iron oxide magnetic nanorings. *J. Am. Chem. Soc.* **130,** 16968–16977 (2008).
55. Cao, C. *et al.* Magnetic characterization of noninteracting, randomly oriented, nanometer-scale ferrimagnetic particles. *J. Geophys. Res.* **115,** B07103 (2010).

Acknowledgements

We are grateful to our colleagues in physics, zoology, biology, structural biology and genomic research fields for providing support and constructive suggestions, as these were fundamentally valuable and allowed us to complete this study. In particular, we thank Z. Xu, S. Chen, H. Cheng, J. Chou, Y. Li and J. Ji. We are grateful to GE Healthcare (Sweden) for providing a prototype Superose 6 Increase 10/300 size-exclusion column before commercial launch to separate the Cry/MagR magnetosensor protein complex, which proved to be critical in obtaining a homogeneous sample for EM structural determination. Special thanks to Å. Danielsson, L. C. Andersson, I. Salomonsson, L. Molander and F. Sundberg for technical support on chromatography. We are deeply indebted to P. Hore from University of Oxford for his advice, encouragement and comments on the manuscript. We thank Y. Zhang and Y. Rao for providing total mRNA from *Drosophilia* head and for helpful discussions, E. Zhang for providing Cry cDNAs from mouse and human, and Y. Sun for technical support. We thank F. Zhuang from B. ViewSolid Biotechnology for MagR knocking-out and knocking-down experiments. We also thank Core Facilities at the College of Life Sciences, Peking University, for assistance with EM data collection, and Y. Hu and X. Li for technical support.

Author contributions

C.X. conceived the idea, developed the theoretical framework, and designed the study. P.Z., T.J., S.Q. and C.X. performed the genome-wide screening of MagR candidates. S.Q. did the experimental validation of MagR. S.Q., H. Yin, C.Y. and Y.D. carried out protein purification, EM experiments and crystallization. Z.L. and H.-W.W. did the EM structural analysis. H. Yu and S.-J.L. re-sequenced cryptochromes and MagR genes from monarch butterfly and pigeon. Y.D. and H. Yin performed mutagenesis and model validation. Junfeng H., J.F. and X.Y. conducted antibody preparation and pigeon-retina experiments. Y.H., X.D. performed magnetic measurements and data analysis. Z.Z. and X.D. provided valuable suggestions on physics and navigation systems. C.X. did molecular modelling and data analysis. C.X. and S.-J.L. wrote the paper. All authors commented on the manuscript.

Additional information

Supplementary information is available in the online version of the paper. Reprints and permissions information is available online at www.nature.com/reprints. Correspondence and requests for materials should be addressed to C.X.

Competing financial interests

The authors declare no competing financial interests.

Methods

Summary. The theoretical framework for a biological compass and the predicted features of a putative magnetoreceptor can be summarized as: an iron-binding feature, a gene-expression profile in brain, and the capability of forming a polymeric complex with dCry. The genome-wide search for a magnetoreceptor was carried out and guided by these criteria. After four rounds of *in silico* screening, we did one round of knowledge-based screening and picked out 14 likely candidates for experimental screening. Total mRNA was extracted from *Drosophila* heads and nine out of 14 candidates showed expression in the head. Complex formation with full-length *Drosophila* dCry was validated by co-expression and co-purification in the presence of light and a magnetic field. Only one candidate, CG8198 (Lethal (1) G0136), exhibited stable interactions with dCry and was designated and renamed as MagR. Electron microscopy (EM) was used to determine the structure of the MagR polymer and the Cry/MagR complex as represented by the pigeon (*Columba livia*) magnetosensor. Computational approaches and structural modelling were used to interpret the EM structure and elucidate the mechanism of magnetoreception at the molecular level. The co-localization of clMagR and clCry4 was confirmed by immunofluorescence and confocal laser scanning microscopy in multilayers of the pigeon retina, and the proteins were highly expressed in retina ganglion cells (RGCs). The intrinsic magnetic polarity of the magnetosensor protein complex was proved by EM imaging, a simple purification using iron beads, and protein-crystallization experiments. The magnetic measurements and characterization of clCry4/clMagR were conducted using a Quantum Design magnetic-property measurement system (MPMS-XL1) with a remnant field lower than 4 mG at room temperature.

Genome-wide search for the magnetoreceptor (MagR). We annotated current sets of fly proteins ($n=12{,}536$) using the Gene Ontology (GO) database[56] and each protein was assigned GO annotations describing biological process, molecular function and cellular component. The biological process and molecular function annotations were used for iron-containing protein searching, and 199 proteins whose annotations were relevant to iron were selected (Fig. 2a and Supplementary Table 1). The tissue-specific expression of these proteins was obtained from FlyAtlas[57], and proteins that had a higher expression level in the head (including brain and eyes) than the mean expression value were selected ($n=132$, Fig. 2a and Supplementary Table 2). Membrane integration of proteins was based on GO cellular component annotations and further confirmed by the SMART domain identification tool[58], and proteins with membrane segments were removed from the candidates list (Fig. 2a and Supplementary Table 3). For 98 candidates from the third round of screening, we evaluated the possibility of involvement in magnetoreception and interaction with cryptochrome in an individual manner, based on literature searches and bioinformatics predictions. The top fourteen candidates were then selected for the first round of experimental validation (Fig. 2a and Supplementary Table 4).

Experimental validation and species screening. To confirm the expression of candidates in *Drosophila* head, RT-PCR was performed. A cDNA library from *Drosophila* head was provided by Y. Zhang and Y. Rao (Peking University). Nine out of 14 candidates had strong expression and full-length cDNA was obtained (Supplementary Table 4).

To validate complex formation and interaction with, the known magnetoreception-related protein cryptochrome, double tags and tandem co-purification procedures were used (Fig. 2b). Full-length *Drosophila* dCry and nine magnetoreceptor candidates (Supplementary Table 4) fused with His-tag and strep-II tag at the N-terminal, respectively, were co-expressed in *Escherichia coli* BL21 (DE3) at 15 °C, induced by isopropyl β-D-thiogalactoside (IPTG). The expression of recombinant protein of all constructs (dCry and all candidates) was confirmed by SDS–polyacrylamide gel electrophoresis (SDS–PAGE). For each co-expression combination (dCry and one selected candidate), the soluble fraction of *E. coli* lysis was purified by Ni-NTA affinity chromatography (QIAGEN, Valencia, California) followed by direct application to a Strep-Tactin column (IBA). All purification steps were carried out at 4 °C under blue light in a magnetic field, supplemented with protease inhibitor mix (Roche), and the purification was monitored by SDS–PAGE. Through this double-tag co-expression and co-purification system, only one candidate CG8198 (Lethal (1) G0136) showed stable interactions with dCry (Fig. 2c). For further purification of the magnetosensor protein complex, see details below in the section 'Protein purification for electron microscopy'.

For species screening, full-length cDNA of all copies and isoforms of Cry and MagR from five other species, including monarch butterfly (*Danaus plexippus*), pigeon (*Columba livia*), naked mole rat (*Heterocephalus glaber*), minke whale (*Balaenoptera acutorostrata*) and human (*Homo sapiens*) were synthesized and cloned into expression vectors with His-tag at the N-terminal of Cry and Strep-II tag at the N-terminal of MagR. All possible Cry and MagR combinations in different species were co-expressed and co-purified following the method described above; complex formation was shown in SDS–PAGE. A summary of species screening is shown in Supplementary Table 5, and results from four typical species are selected and shown in Fig. 2c and Supplementary Fig. 3. Only one type of Cry forms a complex with MagR in different Cry and MagR combinations in each species tested, suggesting the specificity of Cry and MagR interactions, as illustrated in Supplementary Fig. 3.

Protein purification for electron microscopy. Based on the species screening, pigeon cryptochrome 4 (clCry4) and MagR (clMagR) were selected for further analysis. As described above, full-length pigeon clCry4 and clMagR genes were synthesized and cloned into an expression vector with His-tag and Strep-II tag, respectively, fused to the N-terminal and co-expressed in *E. coli* strain BL21(DE3). Bacterial cells were harvested after being induced with 20 μM isopropyl β-D-1-thiogalactopyranoside (IPTG) overnight at 288 K and resuspended in lysis buffer (20 mM Tris, pH 8.0, 10 mM 2-mercaptoethanol) with complete protease-inhibitor cocktail and lysed by sonication on ice. After centrifugation, the supernatant was initially purified using a QFF column to remove one major contaminant protein fragment (degradation of clCry4, confirmed by mass spectra). After the QFF column, the fractions of flow-through were collected and loaded onto Ni-NTA matrix; we then washed the matrix with washing buffer (20 mM Tris, 150 mM NaCl, 20 mM imidazole, pH 8.0) about 50 column volumes (CV). After elution from Ni-NTA matrix using elution buffer (20 mM Tris, 150 mM NaCl, 300 mM Imidazole, pH 8.0), proteins were purified followed by Strep-Tactin matrix. After washing the matrix with washing buffer (20 mM Tris, 150 mM NaCl, pH 7.5) about 20 CV, proteins were eluted from Strep-Tactin matrix using elution buffer (20 mM Tris, 150 mM NaCl,5 mM desthiobiotin, pH 7.5).

Size-exclusion chromatography was then used to obtain a homogeneous protein preparation for EM structural determination. A Superdex 200 10/300 column (GE Healthcare) was originally attempted (20 mM Tris, 150 mM NaCl, pH 7.5). The magnetosensor complex eluted near the void volume, and protein aggregation and large protein particles were observed under negative-stained EM. Similarly, the clMagR protein eluted as two peaks, one near the void column and the other eluted as a mixture of dimer and monomer, whereas clCry4 eluted as a mixture of dimer and monomer, consistent with previous reports.

The same protein preparations were loaded on a Superose 6 Increase 10/300 GL column, which has a capacity to separate proteins up to 5,000 kDa. Two distinctive protein-separation peaks appeared for the magnetosensor complex (Fig. 2f), and protein fractions of both peaks were immediately applied to grids after elution (Supplementary Fig. 6). The first peak shows protein aggregation and a cluster of rod-like magnetosensor structures, which may be due to the magnetic force from each protein complex. Isolated rod-like magnetosensor complexes were observed in the second peak, and were used for EM structural determination (Supplementary Figs 6 and 8). As for MagR purification, several peaks appeared on a Superose 6 Increase 10/300 GL column (Fig. 2d), and all were confirmed as MagR by SDS–PAGE. The first peak (labelled as MagR* in Fig. 2d) contains rod-like MagR polymers under EM (Fig. 2e), and the latter peak (labelled as MagR**) is invisible under EM, presumably owing to the size and molecular weight (14.5 kDa) of the MagR monomer.

It is worth pointing out that purification procedures in the presence of light (daylight or blue light) and a magnetic field of about 50–60 mT (by putting two magnets around the affinity columns during sample loading and washing steps, but removing the magnets in the elution step) consistently increased the protein yield by up to a factor of two. This observation actually inspired us to develop a simple and straightforward procedure for magnetosensor purification, as described in the section 'Iron beads purification' and in Fig. 5c.

EM structural determination. clCry4, clMagR polymer and Magnetosensor complex fractions were immediately applied to EM grids after elution (Fig. 2d,f and Supplementary Fig. 7a). Preparation of negatively stained samples and image acquisition were carried out as described elsewhere[59]. Protein-particle examination and image acquisition were carried out on a Tecnai G2 20 Twin transmission electron microscope (FEI) operated at 120 kV with a nominal magnification of ×50,000, using a dose of ~30 e^{-} $Å^{-2}$ and a defocus range of −1 to −3 μm. Micrographs were collected on an Ultrascan 4000 charge-coupled device (CCD) camera (Gatan) with a pixel size of 0.427 nm at the specimen. For the magnetosensor complex, 17,993 particles were picked from a set of micrographs using EMAN (ref. 60). We then used IMAGIC (ref. 61) to perform iterative reference-free two-dimensional alignment and classification procedures. This alignment and classification procedure was iterated 15 times to converge into final class averages.

For each representative class average, the particles were randomly apportioned into two equally sized sets, class averages were computed, and the Fourier ring correlation between the two class averages was determined[62]. The resolution is estimated as the radius at which the correlation is 0.5, and ranges between 22 and 25 Å.

Molecular modelling. To interpret the EM structure and elucidate the molecular mechanism of magnetoreception, molecular modelling was used. Given that the eukaryotic full-length Cry crystal structure is available[50], we modelled only the

eukaryotic MagR structure for the subsequent molecular docking and '*in silico*' assembly. A 3D homology model of clMagR was generated based on the bacterial homologous IscA structure (PDB ID:1R94; ref. 49) using Phyre server[63]. The crystal-packing pattern in the IscA structure revealed a double-helical linear assembly with Fe–S clusters located in the middle (Supplementary Fig. 10), which is in excellent agreement with our magnetoreception hypothesis (Fig. 1a,b) and, more importantly, is consistent with the rod-like structure we observed under EM (Fig. 2e,h). We then modelled the magnetosensor 'core' structure (clMagR polymer) following the crystal-packing pattern of IscA (Fig. 3a,b and Supplementary Figs 10b and 11).

The docking of Cry was done manually. The crystal-packing interface and protein–protein interaction pattern in the IscA structure provided insights into Cry–MagR complex formation and therefore could be applied to the molecular assembly of the nanoscale magnetosensor complex. In the IscA crystal structure, the conserved helix–helix interaction forms the main crystal lattice interaction shown in Supplementary Fig. 10. A knowledge-based molecular docking was regulated by this interaction. We took one typical lattice interaction out (Supplementary Figs 10a and 11a), and aligned the two conserved helices from one dCry molecule to the two conserved helices from two neighbouring IscA structures (or MagR models), and the docking was a perfect match between Cry and MagR with no space constraint (Supplementary Fig. 11b–d). Therefore, full-length dCry structures were docked onto the rod-like clMagR core structure one by one, and automatically formed a rod-like polymer structure (Supplementary Fig. 11c), fitting the EM structure well (Fig. 3c,d).

Mutagenesis to validate the molecular model. To validate the above structural model, the proposed interface between clCry4 and clMagR was deleted. clCry4 (1-463) with N-terminal His-tag was constructed by removing the C-terminal helix of clCry4 (464–497, corresponding to residues 498–518 in fruit fly dCry, Supplementary Fig. 12a), and co-expressed, co-purified with wild type clMagR by Ni-NTA, followed by Strep-Tactin chromatography. Wild type clCry4 (1-497), clMagR (1-132), and clCry4 mutant (1-463) are expressed and purified respectively as controls to show the molecular weight. Wild type clCry4 and wild type clMagR were co-expressed and co-purified as positive controls to show complex formation (Supplementary Fig. 12b). Another interface in clMagR (1-46) was also deleted in another experiment; however, it abolished the clMagR expression completely (data not shown).

To address the potential roles of the Fe–S cluster in magnetosensor assembly and Cry/MagR interaction, three highly conserved cysteines of clMagR (C60, C124, C126, Supplementary Fig. 12c) were replaced with alanines by site-directed mutagenesis (QuikChange Site-Directed Mutagenesis Kit, QIAGEN). The clMagR cys mutant with N-terminal Strep-II tag was co-expressed and co-purified with clCry4 following the procedures described above. Wild type clCry4 (1-497), wild type clMagR (1-132), clMagR cys mutant (C60A, C124A, C126A), and wild type magnetosensor (clCry4/clMagR) were expressed alone or co-expressed, and purified as controls (Supplementary Fig. 12d). Purified clMagR cys mutant protein was tested for the ability to reconstitute the Fe–S cluster. The absorption spectrum of clMagR cys mutant further confirmed the absence of Fe–S clusters in protein preparation (Supplementary Fig. 12e).

On the basis of our proposed structural model of the magnetosensor, the N-terminal of MagR is tightly packed, with a conserved alpha-helix forming the main interface with Cry. Our results also show that clMagR was purified as two main populations (polymers and mixture of monomers and dimers, Fig. 2d). To validate the assembly pattern of MagR, another expression vector (ProS2-clMagR) with a tag called ProS2 (MW = 24 kDa), inserted after the Strep-II tag and in front of clMagR (Supplementary Fig. 13a), was expressed and purified, as we did with WT clMagR. In contrast to the polymer formation of clMagR, ProS2-clMagR showed only a mixture of monomers and dimers (Supplementary Fig. 13a,b).

All expression vectors described above or elsewhere in this paper are with N-terminal His-tag in Cry or its mutants, and N-terminal Strep-II tag in MagR or its mutants.

Antibody preparation. A New Zealand white rabbit was immunized with 1 mg/1 ml of purified clCry4 mixed with equal volumes of Complete Freund's adjuvant (Sigma) by subcutaneous injection on day 1, and boosted three times with 0.5 mg/0.5 ml clCry4 mixed with equal volumes of Freund's incomplete adjuvant (Sigma) at day 22, day 36 and day 50. On day 60, the whole blood was collected from the immunized rabbit and serum was obtained by centrifugation.

ICR mice were immunized with 0.1 mg/0.2 ml of purified clMagR mixed with equal volumes of Complete Freund's adjuvant (Sigma) by subcutaneous injection on day 1, and boosted with 0.05 mg/0.1 ml clMagR mixed with equal volumes of Freund's incomplete adjuvant (Sigma) on day 22, 0.05 mg/0.1 ml clMagR on day 36 and 0.1 mg/0.2 ml clMagR on day 50 by intraperitoneal injections. On day 60, the whole blood was collected from the immunized mice, and serum was obtained by centrifugation. The specificity of antibodies was validated by western blot with cell lysis expressing clMagR and/or clCry4.

Histological analysis and immunofluorescence analysis. Pigeon retina tissues were dissected and fixed in 10% formalin overnight, rinsed with 70% ethanol, dehydrated in graded ethanol, and embedded in paraffin. Sections (6 μm) were cut and mounted on poly-L-lysine-coated glass slides. After de-paraffinization and hydration, sections were stained with haematoxylin and eosin for histological analysis (Fig. 4m). For immunofluorescence analysis, 6-μm-thick sections were placed in 3% hydrogen peroxide for 20 min and sections were washed three times (5 min/each) in PBS, blocked with normal sheep serum diluted in PBS(1:20). Sections were incubated with rabbit clCry4 polyclonal antibody (diluted 1:500) and mouse clMagR polyclonal antibody (diluted 1:200) with blocking buffer at 4 °C overnight. Sections were rinsed with PBS three times and incubated with donkey Anti-Rabbit IgG H&L (Alexa Fluor 488, 1:200) and donkey Anti-Mouse IgG H&L (Alexa Fluor 594, 1:200) for 2 h at room temperature. Slides were washed in PBS, and nuclei were counterstained with 0.5 mg ml^{-1} DAPI for 30 min at room temperature. Finally, slides were mounted and observed by confocal microscope analysis using an Olympus FluoViewTM FV1000 (Fig. 4a–l).

Orientation analysis. To test the existence of intrinsic magnetic polarity of our purified magnetosensor complex with EM imaging, we prepared protein specimens and EM grids under geomagnetic and artificial magnetic fields (Fig. 5a,b). A sample (EM grids) preparation stage with two replaceable parallel aligned magnets located outside and four replaceable LED lamps on top was designed and customized (Supplementary Fig. 5). The EM grids and specimens were prepared on this stage between a pair of magnets and under LED light. The strength of the geomagnetic field in Beijing, China, was obtained from the National Geophysical Data Center (NOAA; http://www.ngdc.noaa.gov/geomag-web/#igrfwmm) and confirmed by a magnetometer in the laboratory where experiments were carried out. All EM specimens and grids were prepared under the geomagnetic field (about 0.4 Gs, or 0.04 mT) or an external magnetic field (10 Gs, or 1 mT) vertical to the direction of the geomagnetic field. For each grid we punched a hole with a needle in the edge to mark the location of the north pole of the magnetic field, and therefore all the grids could be aligned and loaded into the electron microscope with uniform orientation. About 500 isolated rod-like magnetosensor complex particles for each condition were picked using EMAN (ref. 60). All particles were carefully analysed by orientation and then classified into three groups: parallel (to the magnetic field lines), vertical (to the magnetic field lines) or other (Fig. 5a,b and Supplementary Fig. 14). The orientation preference under different magnetic fields was calculated on the basis of the number of magnetosensor protein particles in each group, each experiment was repeated three times and the standard deviation calculated.

To avoid the potential influence of liquid flow and shear force on particle orientation during EM grid preparation, especially during the washing steps, we absorbed the extra solutions from the grid only from one direction perpendicular to the magnetic field direction. As a control, we also prepared EM grids after absorbing the extra solution from the direction parallel to the magnetic field and did not observe differences in particle orientation, suggesting that the liquid flow effect might be negligible during the grid washing steps.

Iron beads purification. Fe_3O_4–SiO_2 nanoparticles (BeaverBeads) were used to purify the magnetosensor complex from cell lysis. 0.5 ml of *E. coli* BL21(DE3) expressed with clMagR or co-expressed with clCry4 and clMagR was harvested and resuspended in TBS buffer (20 mM Tris, 150 mM NaCl, pH 7.5). The supernatant was incubated with 0.1 ml Fe_3O_4–SiO_2 (10 mg ml^{-1}) for 30 min at room temperature. We removed the supernatant by centrifugation and washed three times with TBS buffer. Absorbed protein was resuspended by adding loading buffer into the nanoparticles and confirmed by SDS–PAGE (Fig. 5c).

Protein purification and crystallization. Pigeon cryptochrome 4 (clCry4) and MagR (clMagR), and monarch butterfly cryptochrome 1 (dpCry1) and MagR (dpMagR) were selected for crystallization experiments. An initial attempt to concentrate purified magnetosensor complex failed, presumably owing to protein aggregation driven by magnetic force. Therefore, Cry and MagR were expressed and purified separately, and then mixed together for crystallization. For this purpose, another construct of MagR was generated and a Strep-II tag, a His-tag and a ProS2 tag followed by a HRV3C protease digestion site were fused to the N-terminal of MagR. The soluble MagR protein was purified by Ni-NTA agarose followed by anion-exchange (HiTrap Q HP column, GE Healthcare). After HRV3C digestion to remove N-terminal tags, high-purity clMagR and dpMagR protein preparations were obtained. As for the His-tagged Cry protein, QFF chromatography followed by a Ni-NTA affinity column, and a size-exclusion Superdex 75 column (GE Healthcare) was used to obtain homogeneous clCry4 (and dpCry1).

Cry proteins (clCry4 and dpCry1) were concentrated to 10 mg ml^{-1} in storage buffer 1 (20 mM Tris, pH 8.0, 150 mM NaCl, 10 mM 2-mercaptoethanol), and MagR proteins (clMagR and dpMagR) were concentrated to 5 mg ml^{-1} in storage buffer 2 (20 mM Tris, pH 7.5, 150 mM NaCl, 10 mM 2-mercaptoethanol). Cry and MagR were mixed at a 1:2 molar ratio and used for crystallization experiments

using the hanging-drop vapour-diffusion method at 293 K. Two types of protein crystals with different morphology appeared in multiple conditions within two weeks, with both showing strong magnetic polarity and responses to an external magnetic field (Fig. 5d and Supplementary Fig. 15). Interestingly, only one brown-to-black crystal existed in one hanging drop in all experiments, whereas many translucent yellowish crystals existed in one hanging drop.

Preparation and characterization of M-HFn nanoparticles. Recombinant human ferritin shells composed of 100% heavy-chain subunits were produced in *Escherichia coli* and further used as a reaction template to synthesize iron oxide nanoparticles as described[64,65]. A 4500 Fe/ protein cage was obtained as previously reported[64].

Direct measurement of the magnetic feature of magnetosensor protein or M-HFn nanoparticles in solution. All magnetic measurements were conducted at room temperature (298 K) on a Quantum Design magnetic property measurement system (MPMS-XL1) with a remnant field lower than 4 mG. The MPMS system integrates a superconducting quantum interference device (SQUID) detection system and a precision temperature control unit inside the bore of a high-field superconducting magnet.

Briefly, pigeon magnetosensor (clCry4/clMagR complex) was purified to homogeneity by QFF followed by Ni-NTA and Strep-Tactin chromatography and then stored in storage buffer (20 mM Tris, pH 7.5, 150 mM NaCl) at 3.8 mg ml^{-1}. The room-temperature magnetization of clCry4/clMagR magnetosensor complex was measured as the function of field, obtained by subtracting the contribution of buffer (Fig. 5e and Supplementary Fig. 16a). A hysteresis loop is observable besides the diamagnetic background, whereas an obvious linear dependence indicates that no ferrimagnetic ordering exists in buffer. Magnetic properties of synthesized magnetite-containing human ferritin (M-HFn) nanoparticles, purified as described above, were used as a control (Fig. 5f and Supplementary Fig. 16b). The obvious linear dependence indicates that no ferrimagnetic ordering exists in M-HFn. All data were collected at 298 K, the maximal external magnetic field $H = 100$ G.

References

56. Ashburner, M. *et al.* Gene ontology: Tool for the unification of biology. The Gene Ontology Consortium. *Nature Genet.* **25,** 25–29 (2000).
57. Chintapalli, V. R., Wang, J. & Dow, J. A. Using FlyAtlas to identify better *Drosophila melanogaster* models of human disease. *Nature Genet.* **39,** 715–720 (2007).
58. Schultz, J., Milpetz, F., Bork, P. & Ponting, C. P. SMART, a simple modular architecture research tool: Identification of signaling domains. *Proc. Natl Acad. Sci. USA* **95,** 5857–5864 (1998).
59. Nishida, N. *et al.* Activation of leukocyte b2 integrins by conversion from bent to extended conformations. *Immunity* **25,** 583–594 (2006).
60. Steven, J., Ludtke, P. R. B. & Chiu, W. EMAN: Semiautomated software for high-resolution single-particle reconstructions. *J. Struct. Biol.* **128,** 82–97 (1999).
61. van Heel, M., Harauz, G., Orlova, E. V., Schmidt, R. & Schatz, M. A new generation of the IMAGIC image processing system. *J. Struct. Biol.* **116,** 17–24 (1996).
62. Saxton, W. O. & Baumeister, W. The correlation averaging of a regularly arranged bacterial cell envelope protein. *J. Microsc.* **127,** 127–138 (1982).
63. Kelley, L. A. & Sternberg, M. J. Protein structure prediction on the Web: A case study using the Phyre server. *Nature Protoc.* **4,** 363–371 (2009).
64. Fan, K. *et al.* Magnetoferritin nanoparticles for targeting and visualizing tumour tissues. *Nature Nanotech.* **7,** 459–464 (2012).
65. Galvez, N. *et al.* Comparative structural and chemical studies of ferritin cores with gradual removal of their iron contents. *J. Am. Chem. Soc.* **130,** 8062–8068 (2008).